Tikrit Journal of Veterinary Sciences (2025) 1(2): 119-133
DOI : 10.25130/tjvs.4.2.14

IRAQI Academic Scientific Journals

TJVS Tikrit Journal of Veterinary Sciences

Tikrit Journal of Veterinary Science

Macroscopic and Histopathological Evaluation of Bioactive Glass–Acacia Gum Composite for Repairing Critical Radial Bone Defects in Rabbits

[1] Haider F. Salloum, [2] Areeg K. Mahdi

1, 2 Department of Veterinary Surgery and Obstetrics, College of Veterinary Medicine, University of Baghdad, Baghdad, Iraq.

ARTICLE INFO.

Article history:
-Received:11/5/2025
- Received In Revised Form:20/7/2025
-Accepted: 31/ 7/2025
-Available online:

Keywords:
Acacia Gum, Bioactive Glass, Bone Defects, Rabbits, Tissue Engineering.

Corresponding Author:
Name:
Haider F. Salloum
E-mail:
haidar.fattah2302m@covm.uobaghdad.edu.iq
Tel:

ABSTRACT

This study assessed the regenerative potential of a bioactive glass–acacia gum composite for repairing critical-sized radial bone defects in rabbits. Under general anaesthesia, a 10mm segmental defect was created in the distal radius. Over 12 weeks macroscopical examination showed proper implant integration in the treated group, with no signs of infection or rejection, while control animals exhibited persistent fibrous tissue and non-union. Histopathologically, the treated group showed early hyaline cartilage and trabecular bone formation with continued ossification and reduced inflammation due to the acacia gum additive which minimized inflammatory response and controlled bioactive glass degradation. In contrast the control group does not heal spontaneously and remains filled with fibrous connective tissue. These results demonstrate that the BG–acacia composite reflecting both osteoconductive and anti-inflammatory properties of the implant and supports reliable bone regeneration and may serve as a promising implant in critical defect repair.

Introduction

Bone defects, especially critical-sized ones, pose significant challenges in veterinary orthopedics due to their limited capacity for natural healing and defects often lead to delayed or non-union, particularly in long bones like the radius (1, 2). Traditional treatments such as autografts and allografts are commonly used but come with drawbacks. Autografts are effective for bone repair but their use is limited by the inadequate availability of donor tissue and the potential complications or morbidity at the donor site (3, 4), while allografts bring a danger of rejection from the immune system and transmission of disease. This has led to increased interest in synthetic alternative materials for soft tissue and bone regeneration (5, 6, 7, 53, 54).

Recent studies reported successful bone regeneration using both synthetic and biological scaffolds. Eggshell hydroxyapatite (8), crab shell nanocomposites (9), and MgO-hydroxyapatite blends (10) showed strong osteoconductivity. Biological materials like swim bladder matrices (11) and xeno-bovine bone (12) also promoted healing in critical defects.

Among synthetic materials, Bioactive glass, which was developed by Larry Hench in the 1960s, has gained attention, particularly the 45S5 formulation that is known for its osteoconductivity and ion-releasing bioactivity (13, 14). However, its amorphous silicate structure and lack of plasticity contribute to its brittleness which limits its mechanical strength, especially in load-bearing sites (15). To overcome this, natural polymers like Acacia gum have been used to form composites that improve stress distribution and reduce fragility. Further enhancements have been achieved by combining Acacia gum with biocompatible agents such as chitosan or gelatin, leading to improved flexibility, degradation control, and cellular response (16).

This study was designed for the purpose of evaluating the effectiveness of a bioactive glass–Acacia gum composite in repairing critical radial bone defects in rabbits, using macroscopic and histopathological assessments to compare healing outcomes with untreated controls, providing insights into next-generation bone graft substitutes for veterinary orthopedic applications.

MATERIALS AND METHODS

Ethical Approval

The experiments performed in this study were approved by the local Animal Care and Use Committee, College of Veterinary Medicine, University of Baghdad (Approval No: P.G/315/2025, dated 6 Feb 2025).

Experimental Animals

Thirty adult healthy male rabbits (wt. 1.5±1 kg) were enrolled in the study. All animals underwent baseline clinical screening and were acclimated for 2 weeks in standardized units (30 × 70 × 60 cm) under controlled conditions. Animals were maintained on a standard diet and had unrestricted access to clean water. Prophylactic antiparasitic management was implemented via a subcutaneous injection of Ivermectin (0.2 mg/kg) to ensure optimal health status.

Experimental Design

Thirty experimental rabbits were randomly divided into two groups (n=15). A 10 mm longitudinal segmental defect was surgically created in the distal portion of the left radius of each animal. In control group was left untreated defect, while the treated group received a bioactive glass implant. Both groups were evaluated at 4, 8, and 12 weeks postoperatively through macroscopic and microscopic assessments to monitor bone regeneration and defect bridging.

Fabrication of bioactive glass

The bioactive glass was synthesized based on the standard [45S5] Bioglass® composition (45 wt% SiO_2, 24.5 wt% Na_2O, 24.5 wt% CaO, and 6 wt% P_2O_5) (Table 1), consistent with the formulation used by (17). Raw materials were homogenized (Fig. 1 A) and melted in a graphite crucible at 1200°C for one hour (Fig. 1 B) a temperature validated for bioglass systems by (18). The molten mixture was rapidly quenched to prevent crystallization, and the resulting glass was manually ground into a fine powder. A solution of acacia gum was prepared according to the described method by (19), where (20g) of acacia powder was dissolved in (100ml) of distilled water and then stirred at room temperature using a magnetic stirrer to form a 5% w/v solution (Fig. 1 C). This solution was then combined with bioactive glass powder to form a paste, which was molded and compressed using a manual hydraulic press (Fig. 1 D) then take the implant out then contoured to conform the appropriate size (Fig. 1 E) that fitted with the defect and dry it by oven in 150°C to form bioactive glass implants and sterilized using ultraviolet (UV) light (20). The final product was analysed by Scanning-Electron-Microscopy (SEM) and X-ray-Diffraction (XRD) to assess its microstructure and crystallinity.

Tikrit Journal of Veterinary Sciences (2025) 1(2): 119-133
DOI : 10.25130/tjvs.4.2.14

Table 1. Ingredients (wt%) and amount of powder (in grams) required for a 100 g batch of BG.

Name	Composition (wt%)	Quantity of powders (g)
Silicon dioxide (SiO_2)	45.00	45.00
Sodium carbonate (Na_2CO_3)	24.50	41.87
Calcium carbonate ($CaCO_3$)	24.50	43.70
Phosphorus pentoxide (P_2O_5)	6.00	9.72

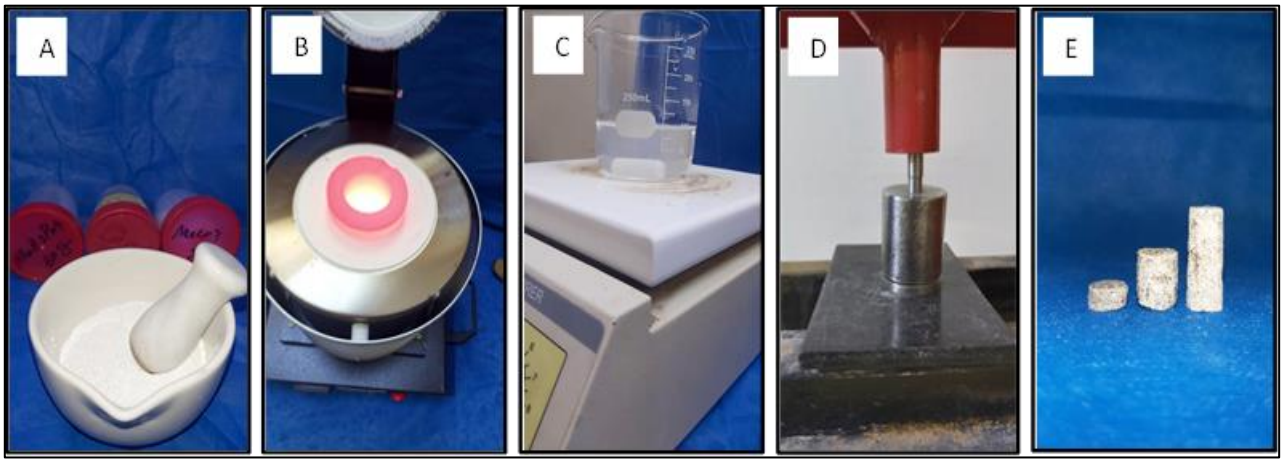

Fig. 1: Photographs show the steps to fabrication of bioactive glass. (A) Grind and mix the materials by mortar and pestle. (B) The powder poured in graphite crucible and melted using high-temperature furnace at 1200C for 1 hr. (C) dissolved acacia powder with DW to prepare Arabic gum (D) pressed the mixture with handheld hydraulic compaction machine (E) bioactive glass implants

Scanning electron microscopy (SEM)

The implant was analyzed by scanning electron microscopy (Axia-chemi-SEM \Thermo-scientific©), at Al-khora for general trading for nanotechnology analysis. The size of the samples used in SEM was (3mm*3mm*10mm). Dried samples were wrapped in aluminum SEM sample mounts (Electron Microscopy Sciences) and sputter-coated with gold using a sputter coater (Quorum/ Q150 RES) prior to testing. Finally, the samples were examined at 5,000 and 10,000 µm magnifications.

Analysis of X-ray diffraction

In XRD analysis of bioactive glass was done using a diffractometer (Aeris research edition XRD\ Panalytical©). The diffraction analysis was achieved with Cu as radiation source, 40 Kv high voltages, 30 mA current, and a scan speed of 5/ min, to obtain structural information on an atomic scale from materials. The diffraction patterns were obtained in the 2Θ" range from (20° - 70°).

Surgical Procedure:

Anesthetic protocol:

General anesthesia was achieved via intramuscular administration of a ketamine-xylazine combination, consisting of 40 mg/kg ketamine (10%, Alfasan, Netherlands) and 5 mg/kg xylazine hydrochloride (2%, VMD, Belgium) (**1, 21, 22**).

Surgical operation:

All surgeries were performed aseptically with in lateral recumbency. approximately 3-5 cm of skin incision at cranio-medial aspect; The left radial flexor carpi-radialis and extensor carpi-radia-longus was blunt separated then exposed the radius bone **(Fig. 2 A)** and locating the defect and marking the site of osteotomy. A 10-mm segmental defect was created in the distal radius using an electric saw **(Fig. 2 B)**. In the treatment group, the defect was reconstructed using a press-fitted bioactive glass implant **(Fig. 2 C)**, while in the control group, it was left empty. Muscle and skin layers were closed with routinely used absorbable sutures 3/0 PDS **(Fig. 2 D)**.

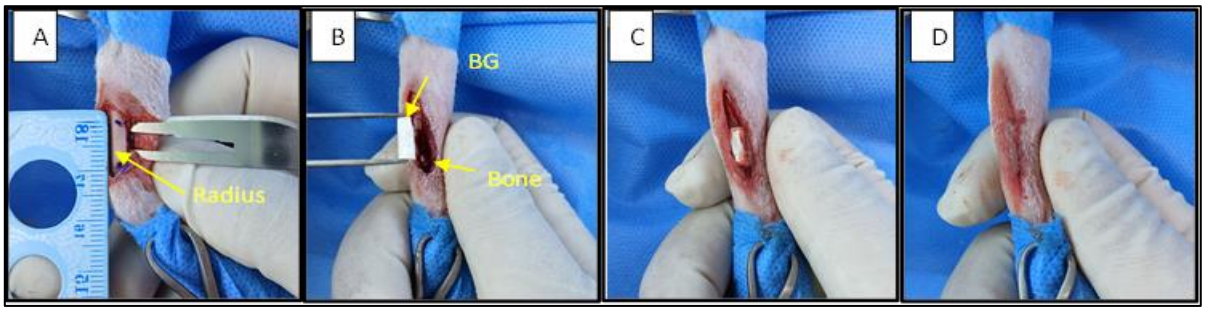

Fig. 2: Photographs show the BG implantation in rabbit radius defect. (A) Marking the bone defect (B) create10-mm radial segmental defect in distal shaft of radius and observation it is dimensional compatibility with BG implant (C) The defect was filled with BG implant in treated group while control group left empty (D) The skin was sutured by subcuticular suture technique.

Postoperative care

The limb was immobilized using gauze and an insulin syringe splint, then secured with adhesive tape to prevent self-trauma. The surgical site was monitored every 48 hours. Ceftiofur sodium (40mg/kg, subcutaneous once daily for 3 days (*Anova*®) and Meloxicam (1.5mg/kg, subcutaneous once daily for 3 days (*Anova*®) were administered for infection control and analgesia. The wound was maintained clean and dry throughout the recovery period.

Macroscopic Examination

The experimental animals were euthanized using a high dose of general anesthesia with ketamine hydrochloride at the end of the 4th, 8th, and 12th week post-operation. The surrounding tissue of the left radius was dissected and examined grossly to assess the degree of bone defect bridging and the integration of the implant with the bone and compered with the bone site of the control group animal that was left empty.

Histopathological Examination

The experimental animals were euthanized using a high dose of general anaesthesia with ketamine hydrochloride at the end of the 4th, 8th, and 12th week post-operation each period had 10 animals euthanized, the histopathological evaluation focused on bone union, implant rejection, and healing stages. Samples were fixed in 10% buffered formalin (10:1 ratio) for 3 days, then decalcified using 10% formic acid with sodium citrate. After confirming decalcification, longitudinal 5µm sections were prepared and stained with haematoxylin and eosin (H and E) for microscopic analysis.

RESULTS and DISCUSSION

RESULTS

Scanning Electron Microscope (SEM)

The SEM analysis of the bioactive glass implant revealed a well-organized, interconnected porous structure with pore sizes ranging approximately from 10 - 90 µm. A broad peak observed in the SEM results further indicated the high purity of the bioactive glass. SEM images showed the presence of partial crystalline surfaces, evidenced it can improve the mechanical strength without greatly affecting the bioactivity (25). The sample also exhibited high porosity and well-interconnected micron-sized pores. These morphological characteristics highlight the material's potential to support cell infiltration and bone tissue regeneration due to its interconnected porosity and optimal pore dimensions. (**Fig. 3**)

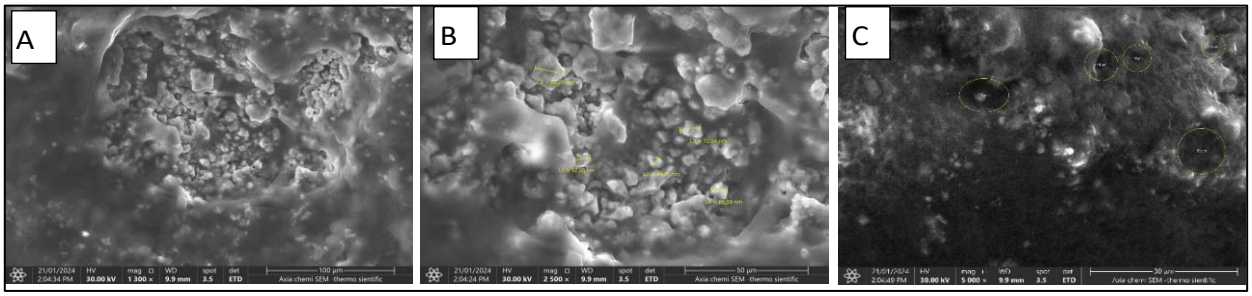

Fig. 3: SEM shows (A), presence of surface crystals. (B) formation a surface with various particle size (C) a well-connected porous structure with pore sizes approximately 10 to 90µm.

Tikrit Journal of Veterinary Sciences (2025) 1(2): 119-133
DOI : 10.25130/tjvs.4.2.14

X-ray Diffraction (XRD)

The XRD analysis, showed that the samples predominantly exhibited an amorphous structure with minor crystalline phases. Distinct diffraction peaks appeared at 2θ values of approximately 22.09°, 24.47°, 30.52°, 34.08°, 36.72°, 40.89°, 43.58°, and 47.65°, corresponding mainly to calcite and sodium-calcium silicate phases. The peak intensities ranged from low to moderate counts, confirming partial crystallinity (Fig. 4).

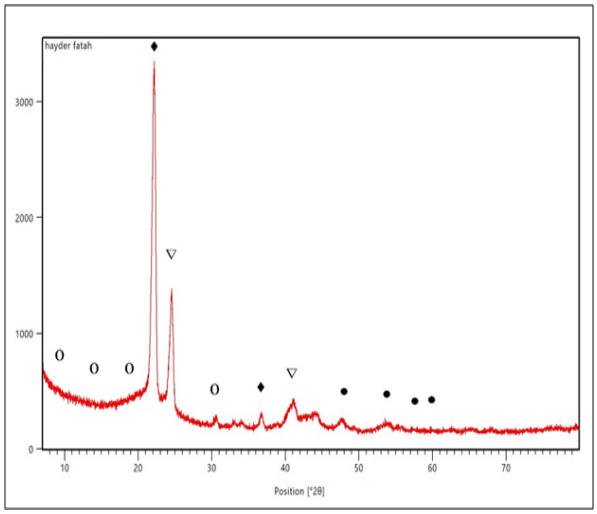

Fig. 4: legend of X-ray diffraction (XRD) pattern of the synthesized bioactive glass. The absence of many sharp peaks and the presence of several hump confirm the amorphous structure of the material, indicating successful rapid quenching during fabrication.

Macroscopic Evaluation

In the control group at early time 4weeks postoperatively, the bone defect gap remained visibly open with minimal bone reaction. There was no evidence formation of newly bone or bridging across the defect site, and the margins were sharply defined. The defect was mainly filled with fibrous tissue, indicating the absence of significant osteogenic activity (**Fig. 5-A)**. While in 8 weeks the size of the bone gap decreased due to partial bridging at the distal edge of the defect. This suggests some biological response with initial phases of the healing cascade, although the defect was continued visibly open, highlighting the insufficient natural healing response in critical-sized defects without intervention (**Fig. 5-B)**. Although at 12 weeks the defect shows incomplete bridging of the defect and continued to be predominantly filled with fibrous connective tissue with slant bridging with the ulna bone, this indicates that full regeneration was not achieved, and the defect remained unhealed, signifying a failure of spontaneous healing to restore the defect within the 12 weeks period (**Fig. 5-C)**. In contrast the treated group at 4 weeks postoperatively the defect was filled with dense BG implant which appeared to occupy the entire gap, this early presence of the material suggests good initial implantation and filling of the defect space and new tissue deposition was noted around the implant, reflecting early osteogenic activity enhanced by the treatment (**Fig. 6-A)**. While in 8 weeks the defect margins appeared less distinct due to new bone deposition and mineralization, and the BG implant showed signs of incorporation into the surrounding bone tissue, indicating early integration and osteoconductive activity (**Fig. 6-B)**. Although at 12 weeks complete bony bridging was achieved, with the defect margins fully obscured with rigid binding between the implant and host bone. This indicates successful defect closure and material integration (**Fig. 6-C)**.

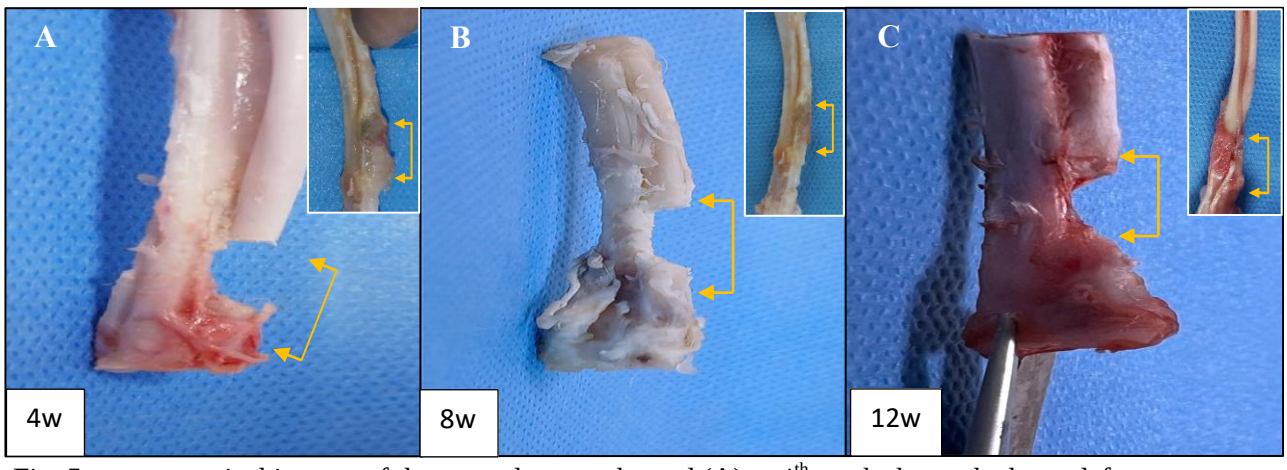

Fig. 5: macroscopical images of the control group showed (A) at 4th week shows the bone defect gap seen visibly with minimum distal reaction. (B) At 8th week, a notable reduction in defect size, with progressive extension from both proximal and distal radial segments toward the centre of the defect. (C) At 12th weeks, the defect area continued to decrease and the bone exhibited toward the ulna where continuity was not achieved leading to the develop of non-union.

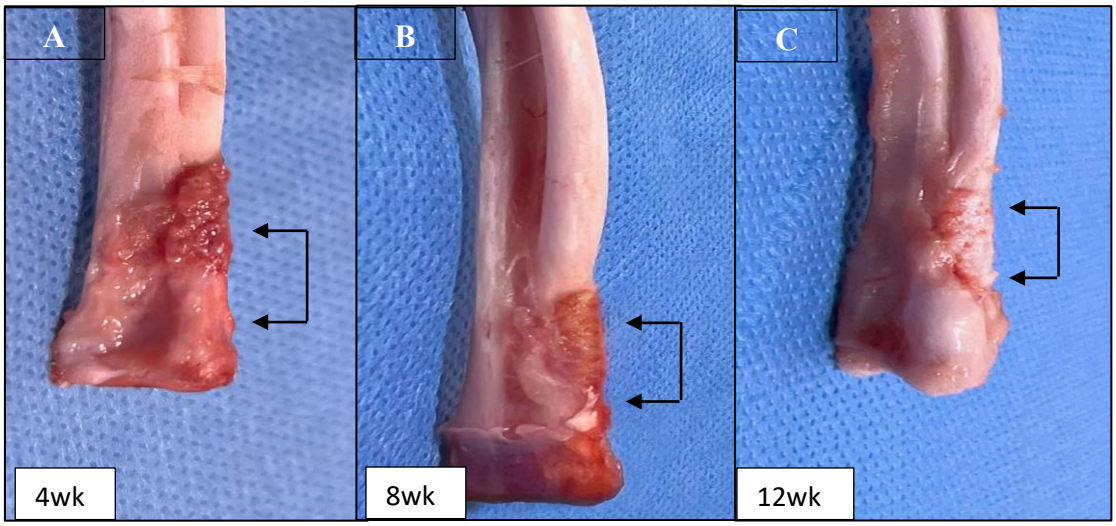

Fig. 6: macroscopical images of the treated group showed (A) at 4th week shows the BG-implant covered with tissue and blood as a result of interaction with the bone edges. (B) At the 8th weeks, the implant's reduced size shows that bone integrates with it and adheres more to the ends of bone defect. (C) at 12th weeks shows the implant is well incorporated with the radius bone and the margin is indistinguishable.

Histopathological Evaluation

Control Group 10-mm

At 4 weeks revealed the presence of loosely organized granulation tissue occupying the entire defect area. The tissue was characterized by dense vascularization with multiple congested capillaries, along with a prominent infiltration of inflammatory cells, including macrophages and plasma cells. Fibroblasts were diffusely distributed throughout the extracellular matrix, indicating an ongoing reparative response. However, no observation of the newly formed bone within the central area of the defect. The margins of the native bone remained clearly demarcated and showed no significant inward growth. There were no signs of osteoblast activity, osteoid deposition, or calcification, and the defect remained in the early inflammatory and proliferative stages of healing **(Fig. 7)**. At 8 weeks, the histological features showed a transition from granulation tissue to dense fibrous connective tissue occupying the defect. Although the inflammatory infiltrate was reduced compared to the 4-week time point, fibroblasts were abundant and embedded in a collagen-rich extracellular matrix. Peripheral regions of the defect demonstrated early trabecular bone formation adjacent to the native bone, but there was no significant extension of these trabeculae into the central defect area. The central core of the defect remained fibrous and avascular, with no signs of osteogenesis or angiogenesis within the central zone. The findings indicate partial wound stabilization, but bone regeneration remained limited to the periphery, failing to bridge the full defect **(Fig. 8)**. At the 12-weeks post-operation, the defect site was mostly filled with dense fibrous connective tissue, with minimal or no vascular structures evident. There was a lack of inflammatory cell infiltration, suggesting that the acute phase of healing had subsided. However, there was no indication of new bone formation within the defect, and the central area remained devoid of osteogenic activity. Peripheral areas showed thin rims of trabecular bone adjacent to the original bone margins, but these structures did not advance into the defect to any appreciable extent. The absence of osteoblasts, osteoid matrix, calcification, or remodelling activity confirmed the failure of spontaneous bone regeneration in this critical-size defect. The overall histological profile is consistent with a non-healing defect, characterized by fibrous tissue encapsulation and permanent structural discontinuity **(Fig. 9)**.

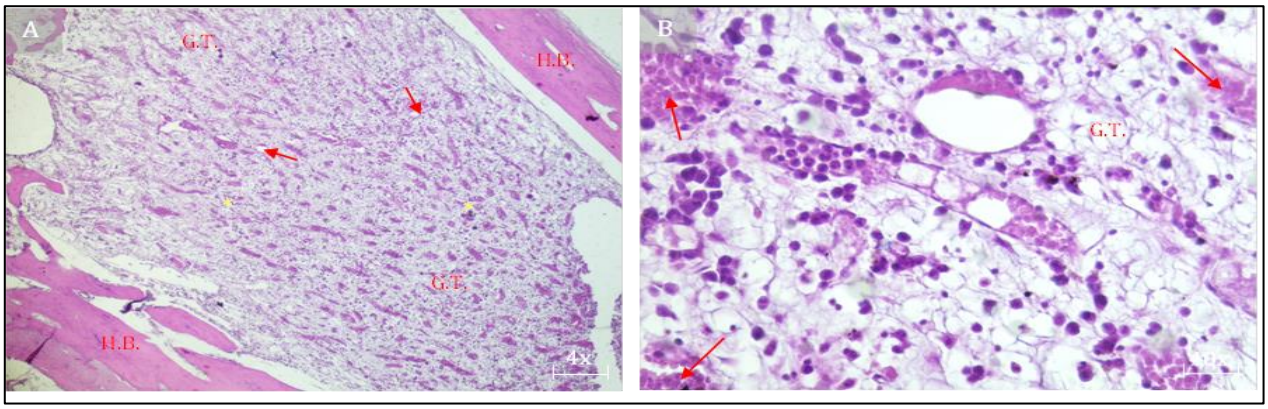

Fig. 7 In control group, at 4th, shows: (A) shows the defect space completely replaced by rich highly vascular granulation tissue filled between two ends of bone (B) infiltrated by moderate mononuclear cell with congested capillaries that filled with inflammatory cell. (400X). GT: granulation tissue\ HB: host bone\ red arrow: congested capillaries\ yellow star: inflammatory cell

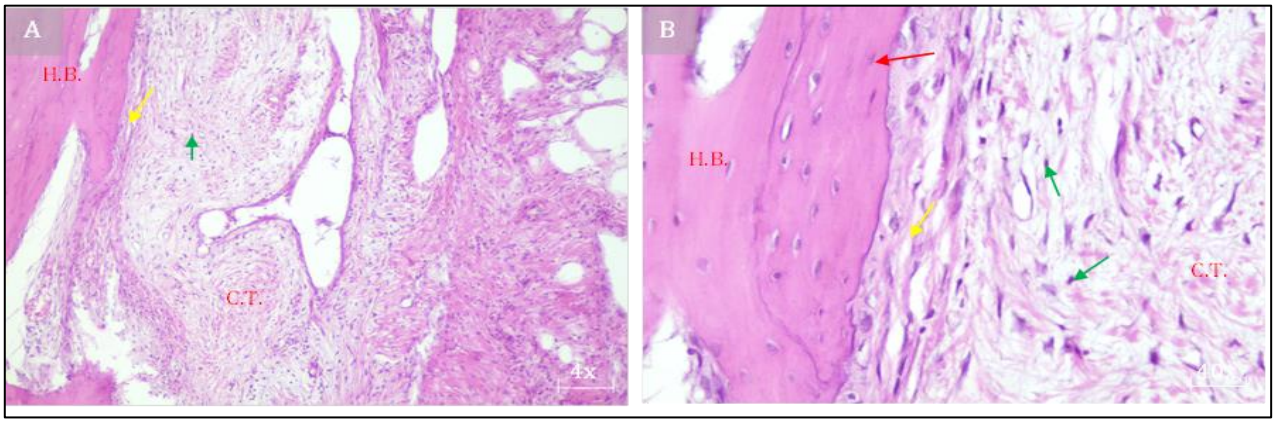

Fig. 8 In control group, at 8th, shows: (A) a large amount of granulation tissue completely bound the space of host bone with (B) an inflammatory response and slight cellular infiltration with scattered irregular newly formed collagen fibers. (400X). CT: collagen fibrous \H.B.: host bone\ yellow arrow: minimal ossification\ green arrow: fibroblast\ red arrow: osteocyte

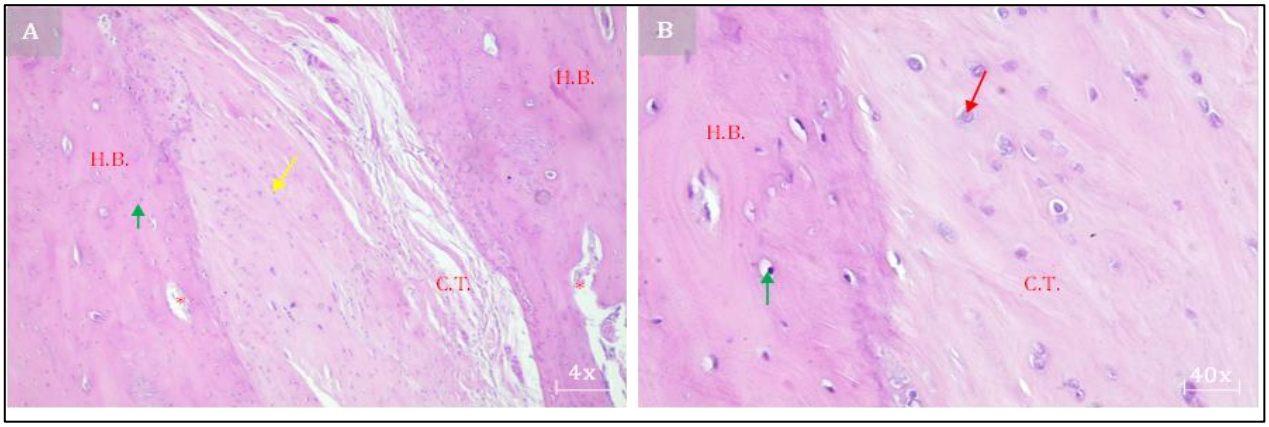

Fig. 9 In control group, at 12th, shows: (A) Mature collagen fibrous connective tissue fills the defect space with sub-peripheral formation of newly formed bone attached to host bone (B) shows remnants of scattered osteocytes with slightly inflammatory cells. (400X). CT: collagen fibrous \H.B.: host bone\ yellow arrow: minimal ossification\ green arrow: osteocyte\ red star: haversian canal

Treated Group 10-mm

At 4 weeks post-operation, histological examination of the treated group revealed the presence of thin, newly formed trabeculae extending into the defect area. These trabeculae were embedded within a matrix rich in immature hyaline cartilage, which occupied a substantial portion of the defect. The cartilage appeared to be undergoing early stages of endochondral ossification, a hallmark of effective bone

regeneration in large defects. Scattered remnants of peripheral marrow tissue were noted, indicating partial preservation of the regenerative microenvironment. The presence of both cartilage and trabeculae indicates a dual pathway of bone repair, combining chondrogenesis with early osteogenesis **(Fig. 10)**. By 8 weeks, the defect area demonstrated clear histological progression toward mature bone formation. The granulation tissue had become more organized and collagen-rich, supporting the formation of new trabeculae, which extended deeper into the defect space. Mature chondrocytes were observed within cartilage islands, further supporting the process of endochondral ossification. Additionally, mononuclear inflammatory cells and multinucleated osteoclasts were present. This cellular activity indicated ongoing remodelling and turnover of the developing bone matrix. These findings align with a transitional phase of healing characterized by both osteogenesis and active tissue remodelling **(Fig. 11)**. At 12 weeks post-operation, the defect area in the treated group was largely filled with thick, well-organized trabecular bone, bridging the defect and integrating with the surrounding native bone. The newly formed bone showed signs of active remodelling, including the presence of osteoblasts lining the trabeculae and scattered osteons in development. Mature chondrocytes persisted in limited zones, suggesting the tail end of endochondral ossification, now giving way to full intramembranous bone formation. Residual granulation tissue was still visible in the periphery, accompanied by moderate mononuclear cell infiltration, reflecting ongoing remodelling. The overall architecture and cellular composition indicated a near-complete regenerative response in a defect that would otherwise fail to heal spontaneously **(Fig 12)**.

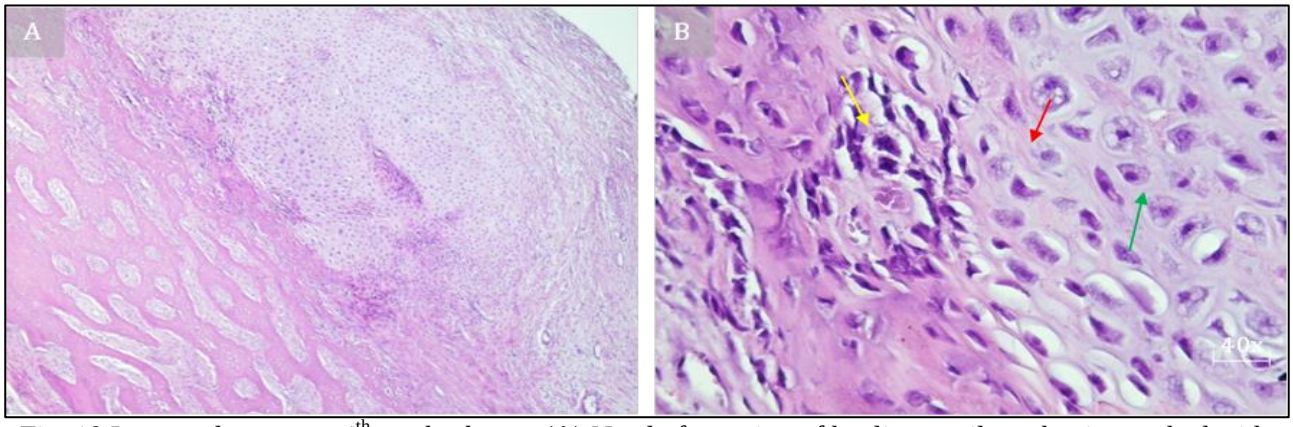

Fig. 10 In treated group, at 4th week, shows: (A) Newly formation of hyaline cartilage that is attached with thin trabecula formation at the site of defect accompanied with a prominent (B) large amount of chondrocytes with remnants of peripheral marrow tissue (400X). Green arrow: hyaline cartilage\H.B.: host bone\ yellow star: trabecular bone\ yellow arrow: marrow tissue\ red arrow: chondrocyte

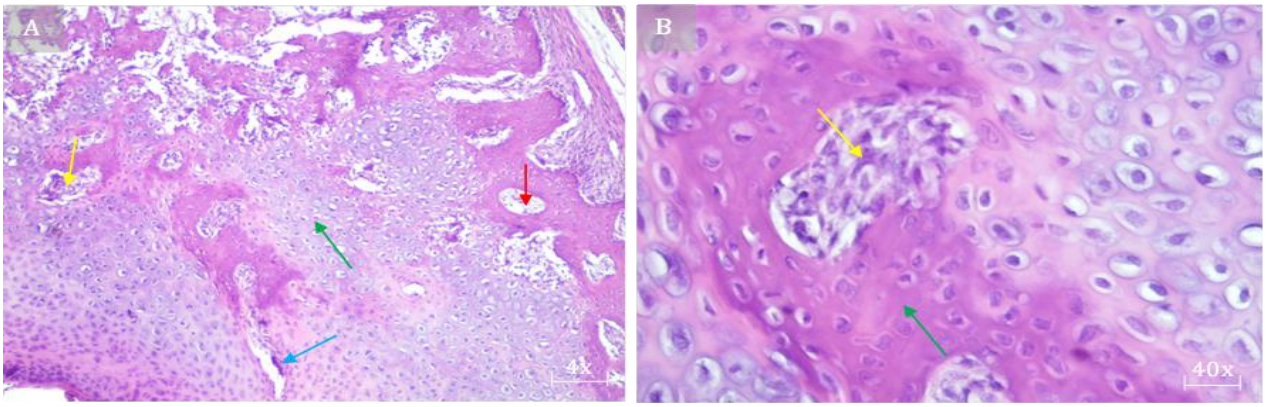

Fig. 11 In treated group, at 8th week, shows: (A) limited woven bone formation at the edge of host bone associated with significant develop persistent mature hyaline cartilage (chondrossification) filled with various develop forms of chondrocyte with (B) infiltrated by mononuclear cells and contain mature hypertrophic chondrocyte adjacent to the host bone with several capillaries. (400X). Green arrow: hyaline cartilage \ orange star: chondrocyte \ yellow arrow: osteoclast\ red arrow: haversian canal\ blue arrow: osteoblast

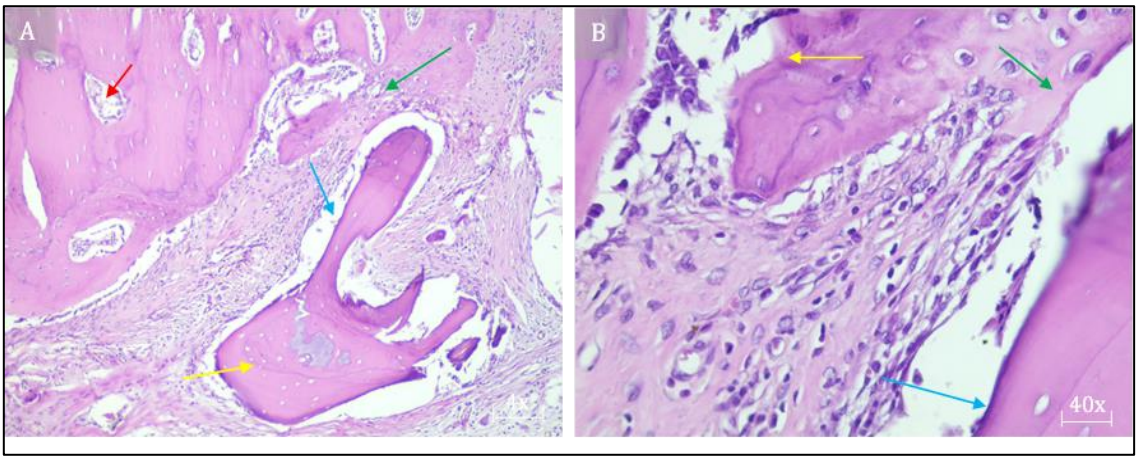

Fig. 12 In treated group, at 12th week, shows: (A) Newly formed thick trabecular bone with fibrous tissue, which is infiltration of numerous mononuclear cells, (B) trabecular bone lining with osteoblast and osteoclast with mononuclear cells. (400X). Green arrow: hyaline cartilage \ orange star: mononuclear cell\ yellow arrow: trabecular bone\ red arrow: haversian canal\ blue arrow: osteoblast \ red triangle: osteoclast

DISCUSSION

The SEM showed that the BG implant had pores of 10-90 µm, which would be the most favourable pore size in agreement to promote the cellular attachment, migration, and ingrowths of tissue. This high-porosity is essential for the initial healing phases, because it permits vascularity and cells infiltration necessary to osteogenesis (23). The interconnected pore structure of the implant also promotes nutrient exchange and neovascularization, which improves biological bonding between the implant and host bone (24). SEM images also showed the structural partial crystallinity, even in the process of a molten-quenched fabrication. This characteristic is probably due to the localized crystallization that occurs during cooling and is not an inconsistency in terms of functionality, but, actually, a useful one, because it can improve the mechanical strength without greatly affecting the bioactivity (25) Although there are some crystalline phases seen in the SEM images, it is well known that some crystallinity in a melt-derived glass can be present as a result of the cooling rate of the melt or slight variation in the glass composition. These crystalline areas support stability and act as nucleation points for bone-like apatite, which is essential for osteointegration. (42). XRD analysis revealed diphase material in which the presence of predominated amorphous phase (broad hump) with weak crystalline diffraction Peaks at around $2\theta \approx$ (22.09°,24.47°,30.52°,34.08°,36.72°,40.89°,43.58 °, and 47.65°). The amorphous silico-phosphate matrix allows bioactivity by ion release (Ca, Na, and P ions), whereas the calcite and sodium-calcium silicates enhance the implant stiffness and mechanical behavior (13, 25, 26). This amorphous-crystalline structure combines mechanical strength and bioactivity, rendering it well-suited for load-bearing bone reconstructive surgeries (15). Bioactive glass surface reacts to release ions like Si^{4+}, Ca^{2+}, Na^{+}, and PO_4^{3-}. These ions are essential in the facilitation of cellular responses such as osteoblast proliferation and differentiation, angiogenesis and ultimately promotion of the bone healing process (15). Especially, the outflow of calcium and phosphate ions leads to fast growing of the hydroxycarbonate apatite layer on the glass surface, which is similar to bone mineral phase. Such a bioactive surface promotes cell attachment and an environment for new bone matrix to form (13, 15). As for the precursor material, acacia gum was chosen because of its multi-functionality. It is also a natural binder, stabilizer, and possibly bioactive material (43) From a chemical point of view, acacia gum carries Ca, Mg and K that can be incorporated either in the bioactive glass matrix or improve its biological behaviour. It also increases the homogeneity of the melt when formed. It is also well known from previous work (44) that the addition of a natural polymer like acacia can improve the dispersion and compatibility of bioactive phase in hybrid composites, this method is innovative because it employs a natural excipient in the melt-derived BG system, which may assist in enhancing its biocompatibility and osteoconductive ability (45). The macroscopic evaluation of untreated 10-mm segmental radial defects over a 12-week observation period consistently demonstrated insufficient healing, underscoring the inherent limitations of natural bone regeneration in critical-sized defects. 4 weeks after surgery, no obvious evidence of defect bridging or new bone

formation was observed; the bone defect was mostly filled with fibrous connective tissue. This observation suggests that osteogenic activity is low and that, according to my interpretation, the defect is larger than the bone's endogenous ability for spontaneous healing which consistent with (27) who found that the untreated critical-sized radial defect left in rabbit featured inert bone ends, and no signs of bone generation after one month. The macroscopic observations at the 8-week stage demonstrated no bridging tissue, and the defect was still filled predominantly with fibrous material, which suggested that only limited repair had occurred. This stasis demonstrated the inability to regenerate spontaneously in large segmental defects which is also a conclusion attained by (30, 28) who showed that these defects need a stimulus from outside for proper healing. After 12 weeks, the macroscopy of the defect indicated a stagnation of the natural healing response, without remarkable further improvement compared to earlier time points. The lack of complete bridging and the degree of unmineralized, fibrous tissue are further support of the fact that critical size defect do not completely heal without assistance. This result is in line with reports from (29), where untreated critical- size long bone defects notoriously failed to heal for prolonged time intervals, with characteristic chronic fibrous non-union patterns.

The treated group showed a significant difference in the healing score compared with that of the untreated group at all time points. At 4 weeks the defect was entirely filled with a solid BG implant that seemed to entirely fill in the defect space. The early appearance of the material reflects the successful implantation and filling of the defect. Also new tissue formation around the implant was found indicating an early osteogenetic activity induced by the treatment (46). I believe this result demonstrates obvious proof of the implant's capacity for establishing a good microenvironment to promote and speed up the beginning of bone formation. The defect rim blurred markedly at 8 weeks, as obvious deposition and mineralization of new bone were observed, and a BG implant started to integrate with the surrounding native bone tissue (47). This reflects the beginning of osteoconductive function and the biological response of the implant to the host tissue. As far as my interpretation goes, these findings indicate that the BG implant is not merely a passive structural filler, but is also functionally involved in the regenerative process by promoting both cell invasion and matrix mineralization. At the 12-week time period, there was no visible defect line, the defect margins were completely hidden, and the bridging appeared solid between the implant and the host bone (48). This demonstrates a closure of the defect and the biological integration of the implanted material, showing a good potential of BG to foster the functional repair of bone at critical sizes (47). In the histologically, the untreated group demonstrated continuous fibrous connective tissue fills the defect space with sub-peripheral formation of newly formed bone attached to host bone with chronic inflammatory reaction, and no osteoblast activity at any time point. This arrested healing is a pattern that is characteristic of the pathologic fibrous non-union as reported by others (31, 32, 33) These findings reconfirm the clinical demand of critical-sized segmental bone defects and the requirement for implant that induce osteogenesis (34, 35, 36). By contrast, the treated group displayed phased and synchronized bone generation. At 4 weeks there were new trabeculae surrounded by immature cartilage suggesting early endochondral ossification which mean the implant encouraging the chondrocyte to infiltration (52) However, relatively preserved marrow architecture was indicative of a favourable microenvironment encouraging osteoprogenitor recruitment and differentiation. This combined chondrogenesis before osteogenesis is in accordance with that reported by (37, 38), who emphasized that the cartilage can be a temporary scaffold for bone in large defects. One important aspect to address regarding histology is the visualization of the implant material. In certain areas, the bioactive glass may appear as voids or unidentified area. This is an artifact of the traditional histological technique processing of inorganic materials. Dissolution of the bioactive glass is possibly due to the decalcification step involving formic acid before sectioning. As reported by (49), powerful acid decalcification agents can breakdown or eliminate inorganic phases, such as calcium silicates, by acid-catalysed degradation, resulting in voids in paraffin-embedded tissue. Furthermore, the staining method H and E does not allow detecting of inorganic substances. As outlined by (51) H and E stains are partly directed towards inorganic cellular and extracellular material; haematoxylin stains nucleic acids but has affinity for basophilic structures, and eosin stains ionizable proteins and molecules but has an affinity for acidophilic structures. On the contrary, the studies by (50) showed that it is possible to extract particles from the implant without degrading the structure of the silica network by using a less aggressive chelating

agent, i.e. EDTA. EDTA processing does make for better visualisation of both mineralised tissues and implanted biomaterials. Despite a lack of these imaging capabilities, the biological response to implanted BG was vividly demonstrated by increased osteoblast activity and new bone formation. These histological observations are in agreement with the gross examination of the tissue prior to decalcification thus lending strong support to the implant osteoconductive and osteoinductive properties (13). By 8 weeks mature chondrocytes and osteoclastic activity indicate active remodelling, an effective sign of bone regeneration. This osteogenic sequence resembles the cellular interplay reported by (39) and is also consistent with previous observations of a dynamic equilibrium between matrix production and matrix degradation during bone healing. Additionally, there is a full integration with host tissue through the hyaline cartilage and newly trabecular bone formation. At 12 weeks, histological sections revealed mature trabecular bone, osteon formation, and bridging of the defect area. There was only minimal cartilage and residual granulation tissue noted at the periphery, indicative of continued angiogenesis and late remodelling. These results are consistent with those reported from (40, 41) who performed comprehensive study on in vivo studies of bioactive glass in critical size bone defect models showing the osteoconductive and osteoinductive properties of bioactive glass and its ability to enable progenitor cells to migrate, attach, and subsequently differentiate into osteoblasts and the in-growth of newly formed bone tissue. In summary, bioactive glass mix with acacia gum - could induce successive bone regeneration in a critical-sized radial defect model. It exhibited a beneficial combination of bioactivity, mechanical stability due to amorphous with partial crystallinity, and open porous structure. the regenerative paraphenomena was clear on the basis of macroscopical and histopathological findings. These results indicate the potential of natural polymer and bioactive glass-based hybrid implant in the context of clinical issues related to large segmental bone defects.

CONCLUSIONS

The present study was conducted to assess the regenerative potential of Bioactive Glass (BG) and acacia gum (AG) in healing critical sized radial bone defects in rabbits. The BG implant possessed good biocompatibility and no side effect were observed. The macroscopically showed bone integration was evident and histopathologically there was evidence of hyaline cartilage and trabecular bone formation indicating osteoconductive and osteoinductive characteristics while the untreated group showed continuous fibrous connective tissue and non-union healing.

ACKNOWLEDGEMENTS

The author would like to express his thanks and grateful to the College of Veterinary Medicine and College of Sciences in Baghdad for providing facilities to complete this study.

References

[1] Mahmood, M. B. (2022). A comparison between ketamine-xylazine and ketamine-midazolam or all of them to induce balance anesthesia in rabbits.
[2] Zhao, M., Zhou, J., Li, X., Fang, T., Dai, W., Yin, W., and Dong, J. (2011). Repair of bone defect with vascularized tissue engineered bone graft seeded with mesenchymal stem cells in rabbits. Microsurgery, 31(2), 130-137.
[3] Kasahara, T., Imai, S., Kojima, H., Katagi, M., Kimura, H., Chan, L., and Matsusue, Y. (2010). Malfunction of bone marrow-derived osteoclasts and the delay of bone fracture healing in diabetic mice. Bone, 47(3), 617-625.
[4] Oryan, A., Alidadi, S., Moshiri, A., and Maffulli, N. (2014). Bone regenerative medicine: classic options, novel strategies, and future directions. Journal of orthopaedic surgery and research, 9, 1-27.
[5] Al-Bayati, A. H., Al-Timmemi, H., and Al-Mudallal, N. H. (2016). Role of acellular bovine urinary bladder submucosa on skin wound healing in Iraqi goats. Iraqi J. Vet. Med, 40(1), 53-60.
[6] Hilal, S., and Hussein, A. K. (2024). Radiological Evaluation of Length Discrepancy and Angular Deformity of Injured Growth Plate in Kit Rabbit Model. The Iraqi Journal of Veterinary Medicine, 48(2), 1-7
[7] Al-Ebadi, A. K., and Al-Bayati, A. H. (2019). Effect of Acellular Bovine Pericardium and Urinary Bladder Submucosa Matrixes in Reconstruction of Ventro-Lateral Hernias in Bucks; Molecular Evaluation. The Iraqi Journal of Veterinary Medicine, 43(1), 67-74.
[8] Atiyah, A. G. and AL-Falahi, N. H. (2019). Egg shell hydroxyapatite implant for repair of radial bone in rabbits. Online Journal of Veterinary Research, 23(6): 606-614
[9] Zebon, S. H., Eesa, M. J., and Hussein, B. F. (2020). Efficacy of nano composite porous 3D scaffold of crab shell and Al-Kharit histological and radiological for bone repair in vivo. The Iraqi Journal of Veterinary Medicine, 44(2), 15-24

[10] Malik, Z. J. and Eesa, M. J. (2022). Effect of magnesium oxide nanoparticles locally or systemic with hydroxyapatite on regeneration of radial fracture in rabbits: radiological study. International Journal of Health Sciences, (I): 10273-10282.
[11] Mahdi, N. A., and Rija, N. H. (2025). Reconstruction of experimentally induced radial bone defect in rabbits by using acellular fish swim bladder and autologous bone marrow clot: Histopathological assessment. Iraqi Journal of Veterinary Sciences, 39(1), 143-154.
[12] Nazht, H. H., Almahmoud, A. M., and Abood, D. A. (2020). Using xeno-Bovine bony implantation as space filler in femoral defect in rabbits. Global Proceedings Repository American Research Foundation.
[13] Hench, L. L. (2006). The story of Bioglass®. Journal of Materials Science: Materials in Medicine, 17(11), 967-978.
[14] Fu, Q., Saiz, E., Rahaman, M. N., and Tomsia, A. P. (2011). Bioactive glass scaffolds for bone tissue engineering: state of the art and future perspectives. Materials Science and Engineering: C, 31(7), 1245-1256.
[15] Jones, J. R. (2013). Review of bioactive glass: from Hench to hybrids. Acta biomaterialia, 9(1), 4457-4486.
[16] Barreto, M. E., Medeiros, R. P., Shearer, A., Fook, M. V., Montazerian, M., and Mauro, J. C. (2022). Gelatin and bioactive glass composites for tissue engineering: a review. Journal of Functional Biomaterials, 14(1), 23.
[17] López Calvo, V., Vicent Cabedo, M., Bannier, E., Cañas Recacha, E., Boccaccini, A. R., Cordero Arias, L., and Sánchez Vilches, E. (2014). 45S5 bioactive glass coatings by atmospheric plasma spraying obtained from feedstocks prepared by different routes. Journal of Materials Science, 49, 7933-7942.
[18] Thonglem, S., Pengpat, K., Rujijanagul, G., Eitssayeam, S., Punyanitya, S., and Tunkasiri, T. (2010). Effects of CaO on properties of P2O5-CaO-Na2O glasses and glass ceramics. Journal of Metals, Materials and Minerals, 20(3), 173-177.
[19] Suliman, R. S., Ali, H., Alamer, A., Aleid, N., Abu-Jafal, A., Abdulgadir, R., and Omer, M. (2020). In vitro Anti-microbial Activity and Wound Healing Evaluation of Acacia Gum Arabia Aqueous Cream. Nat Prod Chem Res, 8, 369.
[20] García-Lamas, L., Lozano, D., Jiménez-Díaz, V., Bravo-Giménez, B., Sánchez-Salcedo, S., Jiménez-Holguín, J., ... and Salinas, A. J. (2024). Enriched mesoporous bioactive glass scaffolds as bone substitutes in critical diaphyseal bone defects in rabbits. Acta Biomaterialia, 180, 104-114.
[21] Al-Haideri, D. H., and Al-Timmemi, H. A. (2024). Efficacy of chitosan nanoparticles and mesenchymal stem cells in rabbit models for sciatic nerve regeneration. Iraqi J. Vet. Sci, 38(2), 369-377.
[22] Eesa, M. J. (2010). Evaluation of general anaesthesia by using Propionylpromazine, Xylazine and Ketamine in rabbits. The Iraqi Journal of Veterinary Medicine, 34(1), 208-217.
[23] Mukasheva, F., Adilova, L., Dyussenbinov, A., Yernaimanova, B., Abilev, M., and Akilbekova, D. (2024). Optimizing scaffold pore size for tissue engineering: insights across various tissue types. Frontiers in Bioengineering and Biotechnology, 12, 1444986.
[24] Bohner, M. (2010). Design of ceramic-based cements and putties for bone graft substitution. Eur Cell Mater, 20(1), 3-10.
[25] Brauer, D. S. (2015). Bioactive glasses—structure and properties. Angewandte Chemie International Edition, 54(14), 4160-4181.
[26] Tilocca, A., and Cormack, A. N. (2011). The initial stages of bioglass dissolution: a Car–Parrinello molecular-dynamics study of the glass–water interface. Proceedings of the Royal Society A: Mathematical, Physical and Engineering Sciences, 467(2131), 2102-2111.
[27] Sharun, K., Pawde, A. M., Manjusha, K. M., Kalaiselvan, E., Kumar, R., and Kinjavdekar, P. (2021). Development of a novel atrophic non-union model in rabbits: A preliminary study. Annals of Medicine and Surgery, 68, 102558.
[28] Wu, C., and Chang, J. (2012). Mesoporous bioactive glasses: structure characteristics, drug/growth factor delivery and bone regeneration application. Interface Focus, 2, 292 - 306.
[29] Zhang, B., Pei, Z., He, W., Feng, W., Hao, T., Sun, M., ... and Zheng, F. (2024). 3D-printed porous zinc scaffold combined with bioactive serum exosomes promotes bone defect repair in rabbit radius. Aging (Albany NY), 16(11), 9625.
[30] Schmitz, J. P., and Hollinger, J. O. (1986). The critical size defect as an experimental model for craniomandibulofacial nonunions. Clinical Orthopaedics and Related Research (1976-2007), 205, 299-308.
[31] Oryan, A., Monazzah, S., and Bigham-Sadegh, A. (2015). Bone injury and fracture healing biology. Biomedical and environmental sciences, 28(1), 57-71.
[32] Wang, Y., Zhang, X., Mei, S., Li, Y., Khan, A. A., Guan, S., and Li, X. (2023). Determination of critical-sized defect of mandible in a rabbit model: Micro-computed tomography, and histological evaluation. Heliyon, 9(7).

[33] Schulze, F., Lang, A., Schoon, J., Wassilew, G. I., and Reichert, J. (2023). Scaffold guided bone regeneration for the treatment of large segmental defects in long bones. Biomedicines, 11(2), 325.
[34] Panteli, M., Pountos, I., Jones, E., and Giannoudis, P. V. (2015). Biological and molecular profile of fracture non-union tissue: current insights. Journal of cellular and molecular medicine, 19(4), 685-713.
[35] Giannoudis, P. V., Einhorn, T. A., and Marsh, D. (2007). Fracture healing: the diamond concept. injury, 38, S3-S6.
[36] Schmidt-Bleek, K., Schell, H., Schulz, N., Hoff, P., Perka, C., Buttgereit, F., ... and Duda, G. N. (2012). Inflammatory phase of bone healing initiates the regenerative healing cascade. Cell and tissue research, 347, 567-573.
[37] Nandi, S. K., Roy, S., Mukherjee, P., Kundu, B., De, D. K., and Basu, D. (2010). Orthopaedic applications of bone graft and graft substitutes: a review. Indian Journal of Medical Research, 132(1), 15-30.
[38] Gerhardt, L. C., and Boccaccini, A. R. (2010). Bioactive glass and glass-ceramic scaffolds for bone tissue engineering. Materials, 3(7), 3867-3910.
[39] Rodan, G. A., and Martin, T. J. (2000). Therapeutic approaches to bone diseases. Science, 289(5484), 1508-1514.
[40] El-Rashidy, A. A., Roether, J. A., Harhaus, L., Kneser, U., and Boccaccini, A. R. (2017). Regenerating bone with bioactive glass scaffolds: A review of in vivo studies in bone defect models. Acta biomaterialia, 62, 1-28.
[41] Ferreira, A. M., Tonda-Turo, C., Mancuso, E., and Gentile, P. (2019). Multilayer nanoscale functionalization to treat disorders and enhance regeneration of bone tissue. Nanomedicine: Nanotechnology, Biology and Medicine, 19, 22-38.
[42] Montazerian, M., Shearer, A., and Mauro, J. C. (2024). Perspectives on the impact of crystallization in bioactive glasses and glass-ceramics. International Journal of Ceramic Engineering and Science, 6(1), e10194.
[43] Mirza, S., Jolly, R., Zia, I., Saad Umar, M., Owais, M., and Shakir, M. (2020). Bioactive gum Arabic/κ-carrageenan-incorporated nano-hydroxyapatite nanocomposites and their relative biological functionalities in bone tissue engineering. ACS omega, 5(20), 11279-11290.
[44] Hadavi, M., Hasannia, S., Faghihi, S., Mashayekhi, F., Zadeh, H. H., and Mostofi, S. B. (2017). Novel calcified gum Arabic porous nano-composite scaffold for bone tissue regeneration. Biochemical and biophysical research communications, 488(4), 671-678.
[45] Khan M, Shah LA, Khan MA, Khattak NS, Zhao H. Synthesis of an un-modified gum arabic and acrylic acid based physically cross-linked hydrogels with high mechanical, self-sustainable and self-healable performance. Mater Sci Eng C 2020;116:111278.
https://doi.org/10.1016/j.msec.2020.111278
[46] Tuusa, S. M. R., Peltola, M. J., Tirri, T., Puska, M. A., Röyttä, M., Aho, H., ... and Vallittu, P. K. (2008). Reconstruction of critical size calvarial bone defects in rabbits with glass–fiber-reinforced composite with bioactive glass granule coating. Journal of Biomedical Materials Research Part B: Applied Biomaterials: An Official Journal of The Society for Biomaterials, The Japanese Society for Biomaterials, and The Australian Society for Biomaterials and the Korean Society for Biomaterials, 84(2), 510-519.
[47] Esfahanizadeh, N., Montazeri, M., Nourani, M. R., and Harandi, M. (2022). Use of bioactive glass doped with magnesium or strontium for bone regeneration: A rabbit critical-size calvarial defects study. Dental Research Journal, 19(1), 18.
[48] Cui, X., Huang, W., Zhang, Y., Huang, C., Yu, Z., Wang, L., ... and Rahaman, M. N. (2017). Evaluation of an injectable bioactive borate glass cement to heal bone defects in a rabbit femoral condyle model. Materials Science and Engineering: C, 73, 585-595.
[49] Savi, F. M., Brierly, G. I., Baldwin, J., Theodoropoulos, C., and Woodruff, M. A. (2017). Comparison of different decalcification methods using rat mandibles as a model. Journal of Histochemistry and Cytochemistry, 65(12), 705-722.
[50] Ranjbar, F. E., Farzad-Mohajeri, S., Samani, S., Saremi, J., Khademi, R., Dehghan, M. M., and Azami, M. (2023). Kaempferol-loaded bioactive glass-based scaffold for bone tissue engineering: in vitro and in vivo evaluation. Scientific Reports, 13(1), 12375.
[51] Fischer, A. H., Jacobson, K. A., Rose, J., and Zeller, R. (2008). Hematoxylin and eosin staining of tissue and cell sections. Cold spring harbor protocols, 2008(5), pdb-prot4986.
[52] Asselin, A., Hattar, S., Oboeuf, M., Greenspan, D., Berdal, A., and Sautier, J. M. (2004). The modulation of tissue-specific gene expression in rat nasal chondrocyte cultures by bioactive glasses. Biomaterials, 25(25), 5621-5630.
[53] Salih, S. I., Al-Falahi, N. H., Saliem, A. H., and Abedsalih, A. N. (2018). Effectiveness of platelet-rich fibrin matrix treated with silver

nanoparticles in fracture healing in rabbit model. Veterinary world, 11(7), 944.
[54] Atiyah, A. G., Alkattan, L. M., and Shareef, A. M. (2024). The radiological study of using fabricated calcium hydroxide from quail eggshell and plasma-rich fibrin for reconstitution of a mandibular bone gap in dogs. Iraqi Journal of Veterinary Sciences, 38(1), 55-62.

Tikrit Journal of Veterinary Sciences (2025) 1(2): 119-133
DOI : 10.25130/tjvs.4.2.14

التحليل العياني والنسيجي لاستخدام الزجاج الحيوي النشط في اصلاح العيوب العظمية الحرجة في عظم الكعبرة لدى الأرانب

حيدر فتاح سلوم [1]، أريج كامل مهدي [2]

1,2 فرع الجراحة والتوليد- كلية الطب البيطري جامعة بغداد- بغداد – العراق.

الملخص

هدفت هذه الدراسة الى تقييم فعالية مركب الزجاج الحيوي مع صمغ الأكاسيا في اصلاح العيوب العظمية الحرجة في عظم الكعبرة للأرانب. تحت تأثير التخدير العام، تم إحداث عيب عظمي بطول 10 ملم في الجزء القاصي لعظم الكعبرة. وخلال فترة امتدت 12 أسبوع، أظهرت الفحوصات العيانية اندماج الغرسة في مجموعة المعالجة، دون وجود علامات عدوى أو رفض، في حين أظهرت الحيوانات في مجموعة السيطرة نسيج ليفي دائم وعدم التحام العظم. من الناحية النسيجية، أظهرت مجموعة المعالجة تكوّن غضروف زجاجي وعظم اسفنجي واستمرار عملية التعظم، مع انخفاض في مستوى الالتهاب بفضل إضافة صمغ الأكاسيا الذي ساهم في تقليل الاستجابة الالتهابية والتحكم في تحلل الزجاج الحيوي على عكس مجموعة السيطرة لم تظهر شفاء تلقائي وبقيت ممتلئة بالأنسجة الليفية الضامة وتوضح هذه النتائج أن مركب الزجاج الحيوي–صمغ الأكاسيا يتمتع بخصائص تحفيزية لتكوين العظم ومضادة للالتهاب، ويدعم تجدد العظم بشكل فعّال، وقد يكون خياراً واعداً في ترميم العيوب العظمية الحرجة.

الكلمات المفتاحية: الزجاج الحيوي النشط، صمغ الأكاسيا، عيوب العظام، الأرانب، هندسة الأنسجة.